IDENTIFY SOLID AND GAS FLOW PATTERNS IN BUBBLING FLUIDIZED BED AND THEIR IMPACT ON SOLID MIXING BASED ON OPERATIONAL CONDITIONS

IDENTIFY SOLID AND GAS FLOW PATTERNS IN BUBBLING FLUIDIZED BED AND THEIR IMPACT ON SOLID MIXING BASED ON OPERATIONAL CONDITIONS

Yunning Li[1], Kai Zhang[2] & Xiangfeng Fan[1]

1 Institute for Materials and Processes, School of Engineering, The University of Edinburgh, Edinburgh EH9 3JL, UK
2 North China Electric Power University, Beijing, 102206, China
x.fan@ed.ac.uk

ABSTRACT

Bubbling fluidization has been widely applied in industrial processes, such as granulation, coating, mixing, power generation from coal, renewable energy production, gasification and pyrolysis. In this study, we attempted to predict solid and bubble flow patterns in a bubbling fluidized bed based on operational conditions, the air distributor and particle velocity, and investigated then the impact of flow pattern on solid mixing behaviour. The solid mixing behaviour was estimated based on the dispersion coefficient of particles, the active index (AI), and the distribution of particle residence time within the entire bed. It was found that the flow patterns are a result of a combination of operational conditions, properties of bed materials, and bed designs. A 'Flow Pattern Parameter (FPP)' was proposed to identify the solid flow pattern in a bubbling fluidized bed. Different flow pattern corresponds to a certain range of the Flow Pattern Parameter. The the particle dispersion coefficient, AI, and the distribution of particle residence time clearly agree with solid flow patterns and bubbling behaviour within the beds.

KEYWORDS

Bubbling fluidization, Flow structure, Mixing, Active index, Solid properties

1. INTRODUCTION

Bubbling fluidization has been employed to many industrial processes, such as granulation, coating and drying, mixing, coal combustion and gasification, renewable energy production, chemical, petrochemical and metallurgical processes [1, 2]. It has been demonstrated that the granulation and mixing efficiency, heat transfer and energy consumption [3, 4] depend on solid/gas flow structure or solid/gas flow pattern. Intensive research has been conducted to investigate the fluidization behaviour experimentally and numerically [5-7], and many models have been developed for optimizing reactor design and bed scale up, and for identifying the effect of operational conditions, particle properties and bed design on fluidization behaviour and mixing. For example, Li et al proposed an energy minimization multi-scale model (EMMS) to characterize the meso-scale structure of fluidization. Xiong et al [7] proposed a smoothed particle hydrodynamics method to solve problems in modelling dense particle–fluid fluidization. Herzog et al [8] used different CFD-codes to predict pressure drop and bed expansion ratio in a gas-solid fluidized bed by considering solid-phase properties, momentum exchange coefficients. Ku et al [9] used an Eulerian-Lagrangian approach to simulate a bubbling fluidized bed and analysed solid flow pattern, bed expansion, pressure drop and fluctuation by considering drag force correlations, particle-particle and particle-wall collisions. Wang et al [10] developed a drag model to simulate the meso-scale structure in solid-gas bubbling fluidized beds. Olsson et al [11] experimentally investigated the fuel dispersion in a large scale bubbling fluidized bed with a cross section area of 1.44 m^2 through analysing the effect of operational conditions and fuel particle properties on the local mixing mechanisms and lateral fuel dispersion. Fotovat et al [12]

investigated the gas distribution in a bubbling fluidized bed and the effect of solid loading and biomass quantity on bubble void fraction and distribution.

However many factors can affect solid/gas flow pattern and solid mixing in a fluidized bed and make fundamental analysis, modelling and prediction of fluidization behaviour difficult and in some cases impossible [13, 14]. All of these factors are interrelated, but we do not know their relative importance. For example, bubbles drive particles, and the moving particles interact with bed wall and packed particles, in turn the interaction between particles and bubbles affect the macroscopic and microscopic behaviour of the bed, bubble size, bubble rise velocity, and bubble distribution.

Solid mixing behaviour in a fluidized bed is usually evaluated in terms of solid dispersion coefficient and various mixing indexes in literature, and the results vary significantly with different techniques used [15-19]. In addition, the dispersion coefficient is usually obtained by fitting one of the two most popular models to the experimental data [20-23, the dispersion model or the counter current backmixing model [24], while both feature some restrictions and limitations [21].

In this study, we use PEPT to directly measure the impact of the operation parameters and air distributor on solid and gas behaviour in a bubbling fluidized bed, and then provide a form of equation to identify the flow structure in bubbling fluidization regime based on bed design and operational conditions. The dispersion coefficients, the distribution of average residence time of the particle at different regions of the bed of particles were calculated based on particle trajectories. An active index (AI) has been developed to evaluate the solid mixing by understanding the frequency and opportunity of particles travelling to different regions within the fluidized beds. The results were analysed and compared with the bubble spatial distribution and solid flow patterns in order to estimate the relationship between solid mixing behaviour and bubble spatial distribution as well as solid flow patterns.

2. MATERIALS AND METHODS

PEPT measurements were carried out using the Birmingham positron camera [25]. The camera comprised of two rectangular gamma detectors with a maximum separation distance of 750 mm. Each detector has an active area of 500×400 mm^2 which can covers the section of bubbling fluidized bed used in this study. The camera can record γ-ray pairs emitted from the labelled tracer particles at a speed up to 100,000 γ-ray pairs per second.

The fluidization experiments were performed in a Plexiglas cylindrical bed. The bed has an inner diameter of 152 mm and a height of 1 m. The bed materials were fluidized by an air flow from a GA11CFF air compressor at ambient temperature. The air flow rate was regulated using calibrated rotameters. Experiments were designed to investigate the effect of the aspect ratio (H/D), superficial gas velocity, and air distributor on solid/gas flow structure. The air distributors were sintered metal sheets with pore diameters varying from 1 μm to 0.23 mm. The bed materials were glass beads with the average diameter of 352 microns, and a size range from 300-400 μm. The density of glass beads was 2700 (kg/m^3). The total mass of the packed bed was 4 kg, 6 kg or 8 kg, which were correspond to the bed aspect ratios of 1, 1.5 and 2 units, respectively. The glass beads used in this study belong to group B in terms of Geldart classification and its minimum fluidization velocity was determined to be 0.15 m/s. The applied superficial gas velocity varied from 0.306 m/s to 0.642 m/s. The experiments were performed within the bubbling fluidization regime that was characterized by visual observation and the measured bed pressure drop.

In order to represent the fluidization behaviour of the bulk material, glass beads with an average size of around 352 μm were randomly selected from the bulk material and radioactively labelled using ^{18}F as tracers [26-28]. In each experiment, we tracked one glass bead. To ensure the measured data representing the behaviour of the bulk and to avoid errors, each experiment was run for 2 hours to

allow the labelled particle passing throughout the bed. The solid flow pattern is plotted based on the average vector graphics using the accumulative tracking data which recorded the particle locations in roughly every 5 milliseconds. As shown in Fig. 1, the experimental set-up consisted of a 3-D gas-solid fluidized bed and the PEPT system.

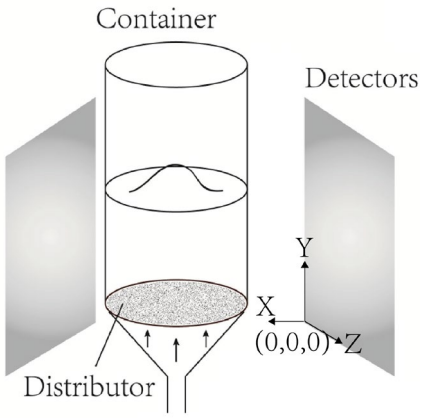

Figure 1. Schematic diagram of the experimental set-up.

In order to represent the fluidization behaviour of the bulk material, glass beads with an average size of around 352 μm were randomly selected from the bulk material and radioactively labelled using ^{18}F as tracers [26-28]. In each experiment, we tracked one glass bead. To ensure the measured data representing the behaviour of the bulk and to avoid errors, each experiment was run for 2 hours to allow the labelled particle passing throughout the bed. The solid flow pattern is plotted based on the average vector graphics using the accumulative tracking data which recorded the particle locations in roughly every 5 milliseconds. As shown in Fig. 1, the experimental set-up consisted of a 3-D gas-solid fluidized bed and the PEPT system.

3. RESULTS AND DISCUSSIONS

Solid flow structure in fluidized beds

PEPT experiments were conducted under various experimental conditions to investigate the effect of air distributors, the bed aspect ratio (H/D), and superficial gas velocities on the solid/gas flow structure in a bubbling fluidized bed. Four flow patterns, which are named as patterns A, B, C and D, were observed in this study as shown in Fig. 2. Patterns A, B and D were observed when the bed material was 300-400 glass beads and the ratio of bed height to bed diameter was unit (Fan et al., 2008a; Fan et al., 2011; Fan et al., 2008b). Pattern C was observed when the ratio of bed height to bed diameter was 1.5 or 2 (Li et. Al., 2014).

Pattern A gave a large circulation cell and covered the whole bed. The glass beads circulated upwards at right-hand side of the bed and moved down to the bottom along the left-hand side. Pattern A was observed when the bed was operated at a low superficial gas with a superficial gas velocity u $\leqslant$ 0.40 m/s, or when the pore size of the air distributor (d_D) was equal or larger than 15 microns. The pattern A has been considered as a poor flow pattern since particles at bottom edge of the bed hardly moved, but it can reveal the effect of the superficial gas velocity, the pore size of air distributors, and the bed aspect ratio (H/D) on solid/bubble flow structures.

Solid flow pattern B has been reported and used frequently to validate the modelling and simulation work in literatures. In pattern B, upward and downwards glass beads were well distributed through the whole cross section of the bed immediately above the air distributor at a relatively uniform velocity. The uniform vertical velocity indicates that the gas travelled up at relative uniform velocity, and the gas distribution and bubble sizes were uniform. At the high layer of the bed, the upward glass beads moved inwards and travelled to the splash zone along the central region. The glass beads always

moved down to the bottom along the bed annulus. Pattern B was observed when glass beads were fluidized at a superficial gas velocity from 0.40 m/s to 0.57 m/s, and the pore diameter of the air distributor was within a range from 60 to 230 microns.

The pattern C was observed in a bubbling fluidized bed when the H/D was from 1.5 to 2 and the pore size of air distributor was 10-60microns. Three solid circulation cells were observed in this pattern. One circulation cell was at the bottom section of the bed, and two circulation cells at the top section. In the intermediate section, the solid flow behaviour was fairly complex. The downward solid flow met with bottom solid flow, resulting in an enhanced mixing and redistribution of the solids to top and bottom sections.

Pattern D was observed when the pore size of the air distributor was less than 10 microns and the H/D was 1-1.5. The fluidized bed can be seen as three sections. The four symmetrical circulation cells were allocated in top section and bottom section. When the air flow was introduced into the fluidized bed, the air drove glass beads moving upwards along the bed annulus, and circulated down in the central region. The tracked glass bead hardly travelled upwards through the central region of the bottom section within the two-hour experiment. Solid flow pattern in the top section of the bed was similar to the flow pattern observed in the pattern B. Glass beads travelled upwards along the central axis of the bed, and then circulated back to the middle section of the bed along the bed annulus. In the intermediate section of the bed, the glass bead flow from the bottom section encountered with the glass bead flow from the top section of the bed in the annulus. The collision of two glass-bead flows pushed particles inwards the bed centre, and enhanced the particle mixing. The collision of two glass flows also split air bubbles to smaller size and gave a longer bubble residence time, therefore enhancing solid-gas contact. After the enhanced mixing, glass beads were redistributed to the bottom circulation and top circulation.

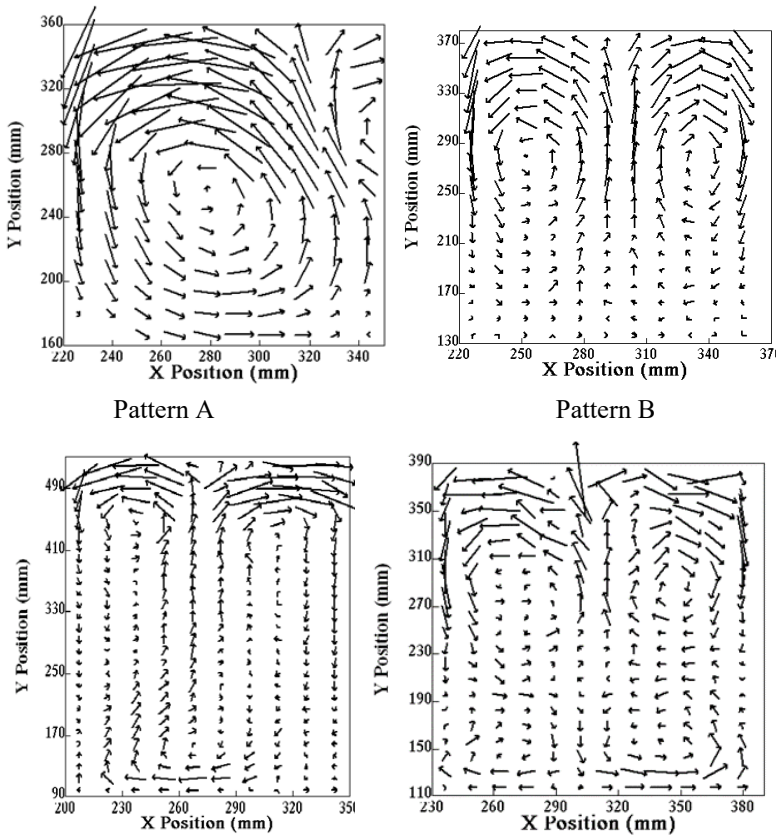

Figure 2. Solid flow structures in bubbling fluidized beds observed by PEPT camera.

Identify Flow Pattern Parameter

The PEPT data have shown that solid flow patterns in a bubbling fluidized bed are controlled by the superficial gas velocity, the bed aspect ratio, and the pore size of the air distributor. Each flow structure is a result of the combination of various factors. In this section, attempts are made to identify the solid flow patterns in a 3D bubbling fluidized bed based on operational conditions, bed design and particle velocity.

In order to find out the conditions under which different flow pattern was formed, a number of PEPT experiments have been conducted to analyse the effects of superficial gas velocity, bed aspect ratio, and the pore size of the air distributors on the flow patterns. The experimental results were then classified into 4 groups based on their flow pattern. In order to identify certain flow patterns for Geldart B particle beds, a 'Flow Pattern Parameter (FPP)' has been proposed based on the PEPT measurement. The FPP takes account of particle kinetic energy, minimum fluidization velocity, superficial gas velocity, the pore size of the air distributor, bed diameter to the bed height ratio. The form of FPP is given as below,

$$FPP = \frac{H_B}{D_B} \cdot \sqrt{\frac{v^2}{d_D^4 \times (u - u_{mf})^2}} = \frac{H_B}{D_B} \cdot \frac{|v|}{d_D^2 \times (u - u_{mf})} \qquad Eq\ (1)$$

Where H_B is the height of the packed bed (mm), D_B is the diameter of the bed (mm), v is the particle speed (mm/s), d_D is the pore diameter of the air distributor (mm), u is the superficial gas velocity (mm/s), u_{mf} is the minimum fluidization velocity (mm/s).

The FPP was calculated based on all experimental data from the fluidized bed with a diameter of 152 mm and packed glass-bead beds of 150-300 mm. Figure 3 shows the relationship between the FPP value and the solid flow patterns. From Figure 3, it can be seen that the solid flow patterns can be clearly separated via FPP, and each flow patterns fall into a specific FPP range. Pattern B can be found when the FPP is greater than 1 but less than 30 ($1/mm^2$). Pattern A can be found when the FPP is between 30 ($1/mm^2$) and 1×10^4 ($1/mm^2$). Pattern C can be found when the FPP is between 1×10^4 ($1/mm^2$) and 4×10^4 ($1/mm^2$), and the pattern D can be found when the FPP is larger than 1×10^6 but less than 1×10^7 ($1/mm^2$).

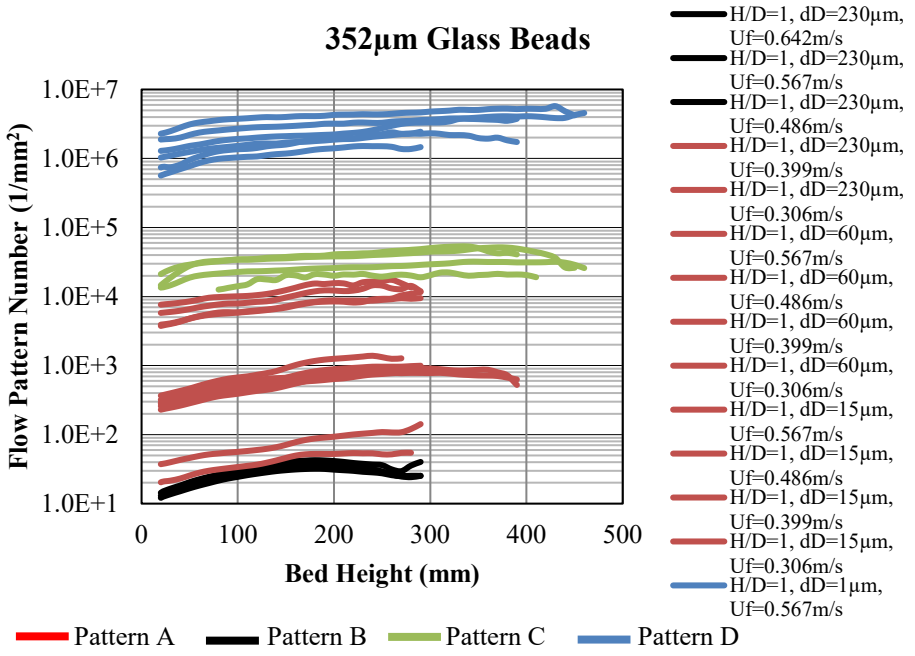

Figure 3. Flow Pattern Parameter vs. bed height for glass beads.

From the FPP expression (equation 1), we can identify a flow pattern in the fluidized bed as long as the FPP value is in the range covered by the required pattern. Figure 4 shows an example for how to identify solid flow pattern based on excess gas velocity ($u-u_{mf}$) when we know the pore size of air distributor. For instance, if the average kinetic energy per unit mass of particles (v^2) is 2.0×10^{-4} $(m/s)^2$, increasing excess gas velocities ($u-u_{mf}$) will results in a decrease in FPP value as well as a change in solid flow pattern. If the pore size of air distributor is 0.001 mm, the pattern will change from D to C. if the pore size of air distributor is 0.01 mm at an excess gas velocity 0.5-0.75 m/s, the pattern will change from C to A. Figure 4 also clearly indicate that the solid flow pattern varies with the pore size of air distributor even though the measured particle kinetic energy is the same. Small pore size gives a large FPP value, therefore, a good flow pattern, good solid/gas contact and solid mixing. Under the same excess gas velocities ($u-u_{mf}$) and the same pore size of the air distributor, higher 'v^2' will results in a slight high FPP value. At the certain average particle kinetic energy (v^2) and a certain pore size, low excess gas velocity gives large FPP value. Overall, the FPP can be potentially developed as a means to identify fluidization behaviour for Geldart B particles within the bubbling regime when the bed aspect ratio is from 1 to 2 units. Further experimental work will be designed to generate a more universal dimensionless FPP number for wide operational conditions and materials, and to remove the particle velocity from FPP number.

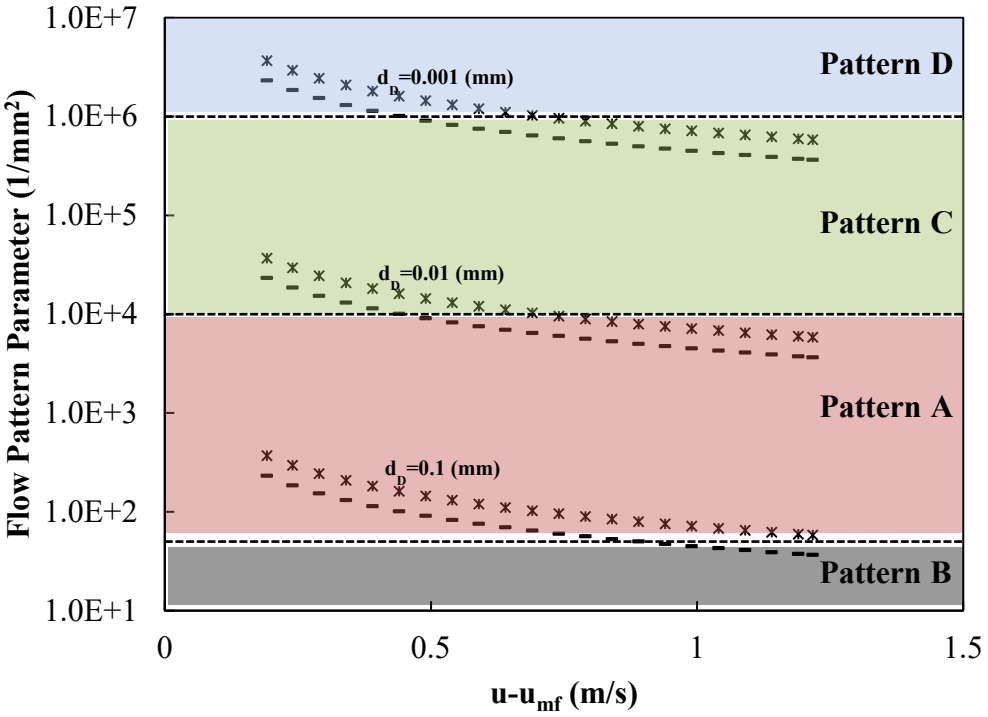

Figure 4. FPP vs. excess gas velocity ($u-u_{mf}$) for a known average kinetic energy of particles, where particle kinetic energy (v^2) for ▬▬ is 2.0×10^{-4} $(m/s)^2$, for ✳✳✳✳ is 5×10^{-4} $(m/s)^2$.

Dispersion Coefficient of Particles

To calculate the dispersion coefficient, the bed was divided into many small compartments and the dispersion of particles was analysed from different positions. Imagining that each passage through this compartment is recorded as an individual particle, "n" passages through this compartment can be assumed to be "n" particles releasing from this position, and the subsequent positions of these "n" particles are the result of particle dispersion. A number of particles (i.e., N=100) were randomly selected from these "n" particles and used as a sample of tagged particles that release from the compartment position at the same time. The subsequent positions of these N particles were followed as if tracking the dispersion of a number of tagged particles simultaneously from the same position. 300 succeeding positions were followed in the present study. The time intervals for each

instantaneous displacement of the N particles were averaged in order to reconstruct the solid dispersion process over time. The dispersion coefficient can then be obtained from the mean squared displacement of the dispersing particles using the Einstein relation, as shown in Equation 2 for the vertical direction (1-D) or Equation 3 for the horizontal direction (2-D) [18, 29], where $S^2(dt)$ is the mean squared displacement at time interval dt, and D is the solid dispersion coefficient.

$$S^2(dt) = 2Ddt \quad \text{(1-D)} \qquad \textit{Eq (2)}$$

$$S^2(dt) = 4Ddt \quad \text{(2-D)} \qquad \textit{Eq (3)}$$

In this study, sample particles are selected randomly, and the dispersion coefficient is determined through standard deviation. Both vertical and horizontal solid dispersion coefficients are measured. This method begins with the calculation of mean squared vertical and horizontal displacements of particles over time. As discussed previously, N particles are released from the starting position (x_0, z_0, y_0) within the fluidized bed at the same time, t_0, as illustrated in Figure 4(a). The next recorded position of each particle is given by (x_{i1}, z_{i1}, y_{i1}), and the time interval between these two successive positions will be Δt_{i1}. Where "i" represents the i^{th} particle and "1" represents the first time step from t_0. As mentioned previously, Δt_{i1} is slightly different for each investigated particle, hence the average will be used to calculate the time when particles travel to their next positions from the releasing point, as given by Equation 4.

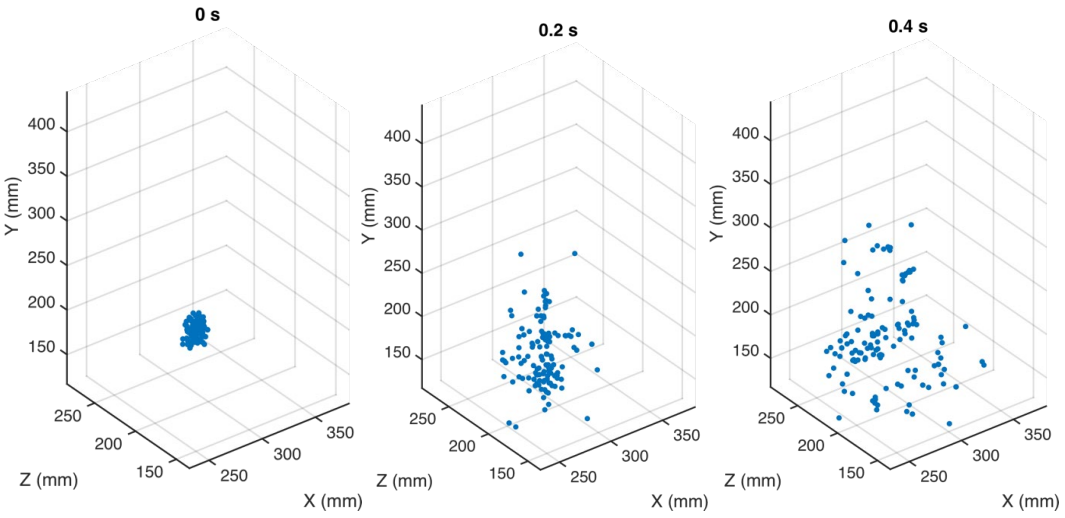

(a) (b) (c)

Figure 5. Dispersion of particles at different times: (a) 0 s; (b) 0.1 s; (c) 0.2 s; (d) 0.3 s; (e) 0.4 s; (f) 0.5 s.

$$t_1 = \frac{1}{N}\sum_{i=1}^{N} \Delta t_{i1} + t_0 \qquad \textit{Eq (4)}$$

At time t = t_1, the mean position of released particles can be calculated from Equation 5, and the vertical and horizontal variances of each particle from the mean position is defined by Equation 6. Then the mean squared displacement or squared standard deviation can be calculated based on Equation 7.

$$\begin{cases} \overline{x_1} = \frac{1}{N}\sum_{i=1}^{N} x_{i1} \\ \overline{y_1} = \frac{1}{N}\sum_{i=1}^{N} y_{i1} \\ \overline{z_1} = \frac{1}{N}\sum_{i=1}^{N} z_{i1} \end{cases} \qquad \textit{Eq (5)}$$

$$\begin{cases} S_{vi}(t_1) = |y_{i1} - \overline{y_1}| \\ S_{hi}(t_1) = \sqrt{(x_{i1} - \overline{x_1})^2 + (z_{i1} - \overline{z_1})^2} \end{cases} \quad \textit{Eq (6)}$$

$$\begin{cases} \overline{S_v(t_1)^2} = \frac{1}{N}\sum_{i=1}^{N} S_{vi}(t_1)^2 \\ \overline{S_h(t_1)^2} = \frac{1}{N}\sum_{i=1}^{N} S_{hi}(t_1)^2 \end{cases} \quad \textit{Eq (7)}$$

The particles will continue dispersing to (x_{i2}, z_{i2}, y_{i2}) at an average time t_2 and with a vertical and horizontal mean squared displacement of:

$$\begin{cases} t_2 = \frac{1}{N}\sum_{i=1}^{N} \Delta t_{i2} + t_1 \\ \overline{S_v(t_2)^2} = \frac{1}{N}\sum_{i=1}^{N} S_{vi}(t_2)^2 \\ \overline{S_h(t_2)^2} = \frac{1}{N}\sum_{i=1}^{N} S_{hi}(t_2)^2 \end{cases} \quad \textit{Eq (8)}$$

Where Δt_{i2} is the time interval of the i^{th} particle between (x_{i2}, z_{i2}, y_{i2}) and the previous position (x_{i1}, z_{i1}, y_{i1}). $S_{vi}(t_2)$ and $S_{hi}(t_2)$ are the instantaneous displacement of the i^{th} particle apart from the particle mean position at $t = t_2$ in the vertical and horizontal directions, respectively.

The calculation is iterated until the mean squared displacement of the released particles becomes stable against time, which means that particles have sufficiently dispersed; the dispersion coefficient of particles in the vertical direction (D_v) and horizontal direction (D_h) can then be determined by Equation 9 from the linear, increasing portion.

$$\begin{cases} D_v = \frac{1}{2} \cdot \frac{d\overline{S_v^2}}{dt} \\ D_h = \frac{1}{4} \cdot \frac{d\overline{S_h^2}}{dt} \end{cases} \quad \textit{Eq (9)}$$

Figure 6 gives the plots of the vertical and horizontal mean squared displacements of particles against time, and the slopes of the linear portion are related to the solid dispersion coefficient. It can be seen that the mean squared displacement increases constantly and nearly linearly over time at the beginning. This is because particles are moving apart from each other and dispersing progressively in the bed. However, after a specific time (i.e., 1-2 s), the mean squared displacement becomes roughly stable against time, which indicates that particles have completely dispersed within the bed and have generated a uniform mixture. The vertical and horizontal dispersion coefficients of the solids can then be obtained according to Equation 8 from the linear slopes in Figure 5.

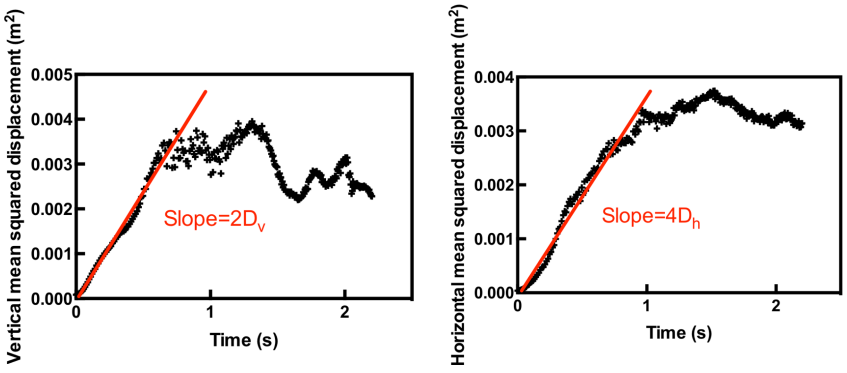

(a) (b)

Figure 6. Mean squared displacement of particles: (a) vertical direction; (b) horizontal direction.

Solid mixing in a fluidized bed is closely related to solid and bubble flow patterns. As shown in Figure 7, the dispersion coefficient is large near the centre and small near the bed wall in both vertical and horizontal directions in pattern A; the vertical dispersion coefficient is uniform over this layer for

patterns B, C and D, while the distribution in the horizontal direction for patterns C and D are more uniform than that for pattern B. The solid horizontal dispersion coefficient for pattern B is large in the centre of the layer and small near the bed wall. The results agree well with the solid flow pattern and bubble behaviours. Comparing the dispersion uniformity and coefficient magnitude (Figures 7) for the four flow patterns in the intermediate section of the bed, the hierarchy of solid mixing has been identified as D > B > C > A in the vertical direction and D > C > A and B in the horizontal direction.

In order to quantitatively evaluate the uniformity of solid dispersion coefficient, the variance (σ^2), of both solid vertical and horizontal dispersion coefficients in the bottom, intermediate, and top sections of the bed for different flow patterns, has been calculated. The results (Figure 8) indicate that patterns C and D have smaller variances than patterns A and B, the uniformity of solid dispersion coefficient is better in patterns C and D than in patterns A and B.

As a result, it can be said that pattern D has the best solid mixing profile among all flow patterns. The vertical dispersion coefficient is always 3-5 times higher than the horizontal dispersion coefficient and dominates the solid mixing. Since particles used to calculate the dispersion coefficients are randomly selected from all particles that passed through the starting point, it is meaningful to assess the deviation between different runs to ensure the reliability of this method. Hence, for each compartment, the calculation of the dispersion coefficients is repeated for 5 runs to investigate the deviation among the dispersion coefficients obtained from these runs. The results indicate that the difference in dispersion coefficients among the 5 runs ranges between 0 and 2.5%, which is very small.

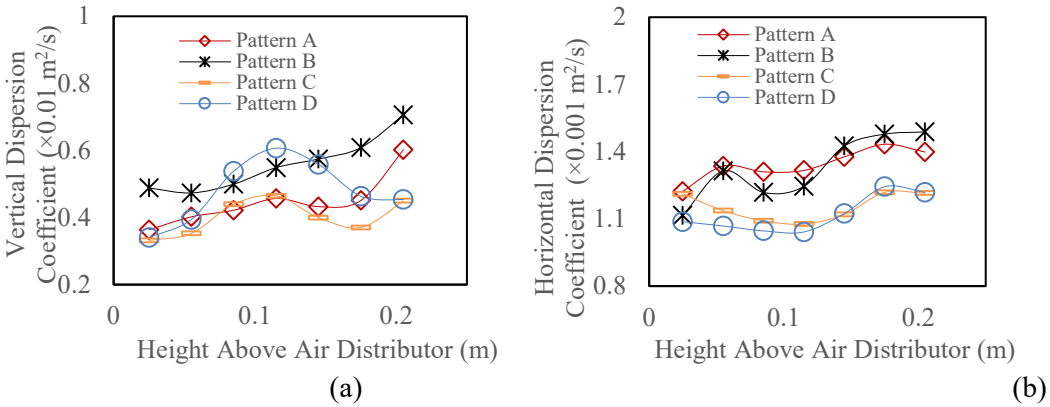

Figure 7. Dispersion coefficients of solids against bed heights: (a) vertical direction; (b) horizontal direction.

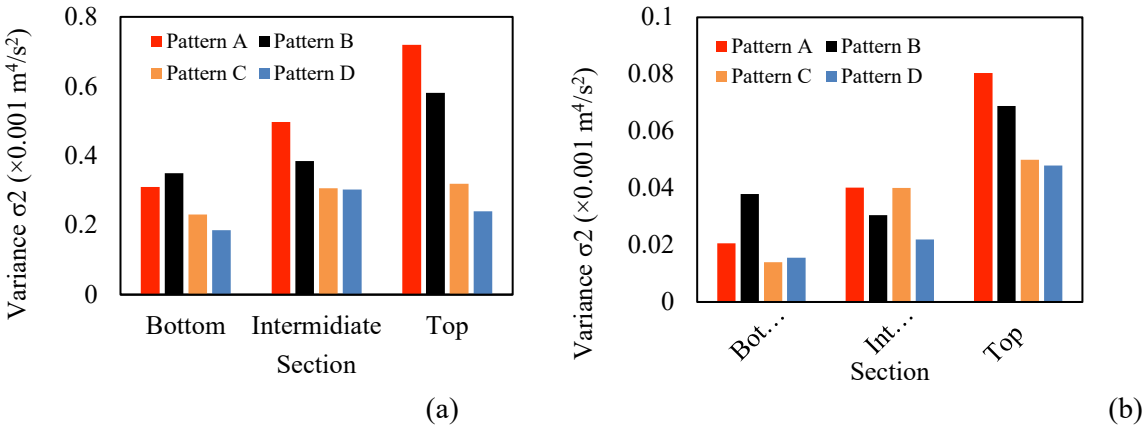

Figure 8. Variance (σ^2) of: a) solid vertical dispersion coefficient, b) solid horizontal dispersion coefficient.

As a result, it can be said that pattern D has the best solid mixing profile among all flow patterns. The vertical dispersion coefficient is always 3-5 times higher than the horizontal dispersion coefficient and dominates the solid mixing. Since particles used to calculate the dispersion coefficients are randomly selected from all particles that passed through the starting point, it is meaningful to assess the deviation between different runs to ensure the reliability of this method. Hence, for each compartment, the calculation of the dispersion coefficients is repeated for 5 runs to investigate the deviation among the dispersion coefficients obtained from these runs. The results indicate that the difference in dispersion coefficients among the 5 runs ranges between 0 and 2.5%, which is very small.

Active Index of Particles

Activity index (AI) is proposed in this study to further evaluate the solid mixing behaviour within fluidized beds. It is defined based on the number of times of particles pass through a unit of volume within a unit of time, as shown in Equation 10. To count the number of times that particles pass through a particular volume, each time the tracer particle falls into a measured volume, its previous location is recorded, and it is considered as an inflow point to the volume. The particle can stay for some time and move to different locations within this volume before it flows out of the volume. Among all the close following positions of the particle from this inflow point, the first position where it is out of this volume will be considered as the successive outflow point from the inflow point for the measured volume, as illustrated in Figure 9. It is understood that if the particle in a region is active, it should flow in and flow out of the region many times. It is also understood that, if the solid mixing is good and particles are fluidized uniformly in a bed, the tracer particle should go everywhere within the bed and has a very similar probability to flow in and flow out of a volume selected from anywhere of the bed. The AI therefore represents the activity of particles in different areas and describes the frequency and probability of particles moving to different locations. For uniform solid mixing, the AI obtained in a different region throughout the entire fluidized bed should have a uniform profile.

$$Activ\ Index = \frac{The\ number\ of\ passes}{Measured\ Volume \times Total\ tracking\ time}\ (/cm^3 \cdot s) \qquad Eq\ (10)$$

In order to determine the AI profile throughout the entire bed, the bed has been divided into many small compartments with the dimension of 10 mm and height of 35 mm. For each compartment, only an inflow with a subsequent outflow of the tracer particle is considered as one pair of entrance, as mentioned previously (Figure 9). An inflow without a subsequent outflow or an outflow missing an inflow of the tracer particle is regarded as an erroneous count and is then discarded from the original data to make the new trajectory data smooth. Once all pairs of entrance have been taken into account from the entire time-position data of the tracer particle, the number of pairs is divided by the compartment volume and the total tracking time of the new smooth data in order to determine the AI value. In order to investigate the effect of solid flow patterns on AI and solid mixing, the AIs are averaged for each layer and a mean value is obtained as a function of bed height. The results for different flow patterns are presented in Figure 10. The overall AI for the 4 patterns decreases in the order of D > C > A and B. This indicates that particles in pattern D are more active and have a similar probability to visit every compartment in the bed. The small AIs obtained in different regions of the bed in pattern A and B show that particles may stay in specific locations rather than moving frequently to different regions.

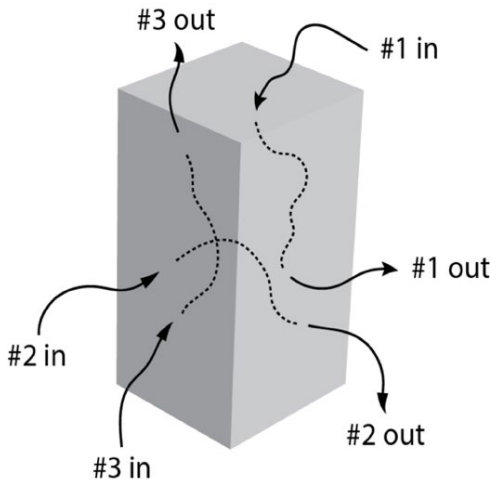

Figure 9. Definition of the pairs of entrance.

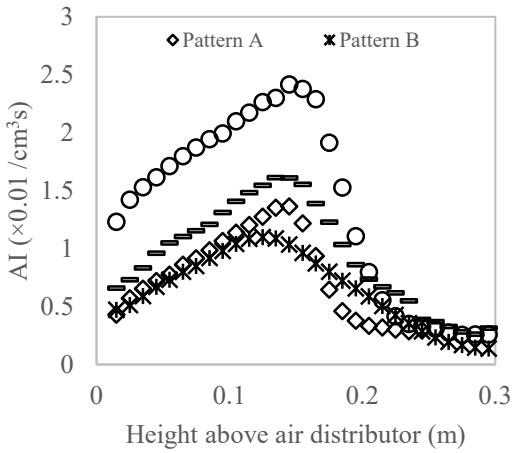

Figure 10. Averaged AI against bed heights.

Residence Time Distribution of Particles within the Bed

In addition to the AI, the residence time of solids in a particular area is an important factor in fluidized beds. To determine the distribution of the particle residence time throughout the entire bed, the bed is partitioned into many compartments using the same manner described previously for determining the AI. For each compartment, once a pair of entrance has been detected, the time interval between the inflow and outflow is calculated and recorded. After all pairs of passes have been determined for a compartment, the average residence time for every entrance of the tracer particle in this compartment is calculated. The obtained average residence time of tracer particle is then divided by the compartment volume to calculate the average residence time per unit volume (s/m^3) of the tracer particle at this position. Figure 11 indicate that particles in patterns C and D are much more active than those in patterns A and B.

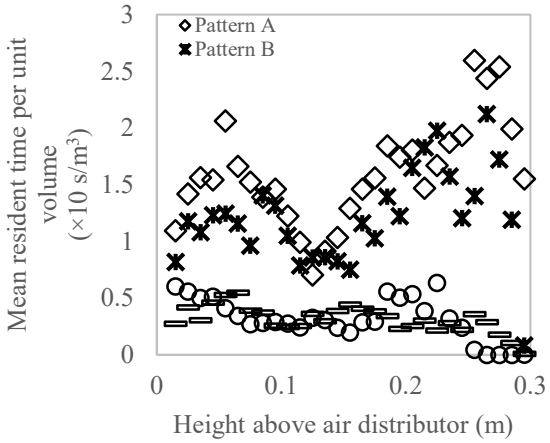

Figure 1. Mean residence time per entrance per unit volume.

4. CONCLUSIONS

The flow patterns in a fluidized bed are a result of a combination of operational conditions, properties of bed materials, and bed designs. A 'Flow Pattern Parameter (FPP)' proposed can clearly identify the flow pattern in a bubbling fluidized bed. The FPP combines the effect of particle kinetic energy, minimum fluidization velocity, the superficial gas velocity, the pore size of air distributor, the bed aspect ratio (H/D). However, the FPP presented here is still at its initial stage. Further development is required to generate a more universal dimensionless FPP number for wide operational conditions and materials.

The solid mixing in bubbling fluidized beds can be evaluated based on dispersion coefficients, AI and particle residence time distributions, which are calculated estimated based on tracer particle trajectories/solid motions. Typically, the solid vertical dispersion coefficient is 3-5 times larger than the horizontal dispersion coefficient and dominates the solid mixing. The AI describes the frequency and opportunity of particles moving to different locations within the bed. It reveals that the expanded bed height of pattern A is lower than other flow patterns. The average AI for pattern D is close to 0.02 /(cm^3s), which is greater than 0.01 /(cm^3s) for pattern C. The average AI for patterns A and B is less than 0.01 /(cm^3s). The average particle residence time throughout the entire bed for patterns C and D is less than 5 s/m^3, and has a uniform value along the bed heights. Conversely, the average particle residence time for patterns A and B is greater than 10 s/m^3 and varies significantly along the bed heights.

REFERENCES

[1] F.P. Di Maio, A. Di Renzo, V. Vivacqua, Extension and validation of the particle segregation model for bubbling gas-fluidized beds of binary mixtures, Chemical Engineering Science 97 (2013) 139-151.

[2] E. Sette, D. Pallarès, F. Johnsson, F. Ahrentorp, A. Ericsson, C. Johansson, Magnetic tracer-particle tracking in a fluid dynamically down-scaled bubbling fluidized bed, Fuel Processing Technology, 138 (2015) 368-377.

[3] Y.R. He, H.L. Lu, Q.Q. Sun, L.D. Yang, Y.H. Zhao, D. Gidaspow, J. Bouillard, Hydrodynamics of gas-solid flow around immersed tubes in bubbling fluidized beds, Powder Technology, 145 (2004) 88-105.

[4] K. Shibata, M. Shimizu, S.-i. Inaba, R. Takahashi, J.-i. Yagi, Pressure Loss and Hold-up Powders for Gas-Powder Two Phase Flow in Packed Beds, ISIJ International, 31 (1991) 434-439.

[5] N. Herzog, M. Schreiber, C. Egbers, H.J. Krautz, 2012. A comparative study of different CFD-codes for numerical simulation of gas-solid fluidized bed hydrodynamics, Computers & Chemical Engineering, 39 (2012) 41-46.

[6] A.D. Salman, M.J. Hounslow, Fluidized bed applications – Preface, Chemical Engineering Science, 62 (2007) 1-1

[7] Q.G. Xiong, L.J. Deng, W. Wang, W. Ge, SPH method for two-fluid modeling of particle-fluid fluidization, Chemical Engineering Science, 66 (2011) 1859-1865.

[8] N. Herzog, M. Schreiber, C. Egbers, H.J. Krautz, A comparative study of different CFD-codes for numerical simulation of gas-solid fluidized bed hydrodynamics, Computers & Chemical Engineering 39 (2012) 41-46.

[9] X.K. Ku, T. Li, T. Lovas, Influence of drag force correlations on periodic fluidization behavior in Eulerian-Lagrangian simulation of a bubbling fluidized bed, Chemical Engineering Science, 95 (2013) 94-106.

[10] Y. Wang, Z. Zou, H. Li, Q. Zhu, A new drag model for TFM simulation of gas–solid bubbling fluidized beds with Geldart-B particles, Particuology, 15 (2014) 151–159.

[11] J. Olsson, D. Pallares, F. Johnsson, Lateral fuel dispersion in a large-scale bubbling fluidized bed, Chemical Engineering Science, 74 (2012) 148-159.

[12] F. Fotovat, J. Chaouki, J. Bergthorson, The effect of biomass particles on the gas distribution and dilute phase characteristics of sand–biomass mixtures fluidized in the bubbling regime, Chemical Engineering Science, 102 (2013) 129-138.

[13] L.M. Garcia-Gutierrez, A. Soria-Verdugo, N. Garcia-Hernando, U. Ruiz-Rivas, Simulation of object motion in a bubbling fluidized bed using a Monte Carlo method, Chemical Engineering Science, 96 (2013) 26-32.

[14] J.A. Laverman, X. Fan, A. Ingram, M.V. Annaland, D.J. Parker, J.P.K. Seville, J.A.M. Kuipers, Experimental study on the influence of bed material on the scaling of solids circulation patterns in 3D bubbling gas-solid fluidized beds of glass and polyethylene using positron emission particle tracking, Powder Technology, 224 (2012) 297-305.

[15] N. Mostoufi, J. Chaouki, Local solid mixing in gas-solid fluidized beds, Powder Technology, 114 (2001) 23-31.

[16] J. Sánchez-Prieto, F. Hernández-Jiménez, L.M. Garcia-Gutierrez, A. Soria-Verdugo, Experimental study on the characteristic mixing time of solids and its link with the lateral dispersion coefficient in bubbling fluidized beds, Chemical Engineering Journal 307 (2017) 113-121.

[17] E. Sette, T. Berdugo Vilches, D. Pallarès, F. Johnsson, Measuring fuel mixing under industrial fluidized-bed conditions – A camera-probe based fuel tracking system, Applied Energy, 163 (2016) 304-312.

[18] M.G. Stein, Particle motion in fluidised beds, PhD thesis, in: University of Birmingham, UK, 1999.

[19] Y. Zhang, C. Lu, M. Shi, Evaluating solids dispersion in fluidized beds of fine particles by gas backmixing experiments, Chemical Engineering Research and Design, 87 (2009) 1400-1408.

[20] J.S. Dennis, Properties of stationary (bubbling) fluidised beds relevant to combustion and gasification systems, in: Scala, F. (Ed.), Fluidized Bed Technologies for Near-Zero Emission Combustion and Gasification. Woodhead Publishing, (2013) 77-148e.

[21] U.Y.V. Lam Cheun Solids motion in fluidised beds of fine particles, PhD thesis, in: University of Birmingham, UK, 2010.

[22] D. Liu, X. Chen, Lateral solids dispersion coefficient in large-scale fluidized beds, Combustion and Flame, 157 (2010) 2116-2124.

[23] J. Sánchez-Prieto, F. Hernández-Jiménez, L.M. Garcia-Gutierrez, A. Soria-Verdugo, Experimental study on the characteristic mixing time of solids and its link with the lateral dispersion coefficient in bubbling fluidized beds, Chemical Engineering Journal, 307 (2017) 113-121.

[24] J.J. van Deemter, Mixing, in: Davidson, J.F., Clift, R., Harrison, D. (Eds.), Fluidization, 2nd ed. Academic Press, Inc., London, England, (1985) pp. 331-355.

[25] X.F. Fan, Z.F. Yang, D.J. Parker, B. Armstrong, Prediction of bubble behaviour in fluidised beds based on solid motion and flow structure, Chemical Engineering Journal, 140 (2008) 358-369.

[26] X. Fan, D.J. Parker, M.D. Smith, Enhancing F-18 uptake in a single particle for positron emission particle tracking through modification of solid surface chemistry, Nuclear Instruments & Methods in Physics Research Section a-Accelerators Spectrometers Detectors and Associated Equipment, 558 (2006) 542-546.

[27] X. Fan, D.J. Parker, M.D. Smith, Labelling a single particle for positron emission particle tracking using direct activation and ion-exchange techniques, Nuclear Instruments & Methods in Physics Research Section a-Accelerators Spectrometers Detectors and Associated Equipment, 562 (2006) 345-350.

[28] X. Fan, D.J. Parker, Z. Yang, J.K.P. Seville, X. Fan, D.J. Parker, Z. Yang, J.K.P. Seville, A Simple and Selective Method for Separation of Trace 61Cu from Nickel Solutions, Nuclear Medicine and Biology, 33 (2006) 939-944.

[29] D.J. Parker, A.E. Dijkstra, T.W. Martin, J.P.K. Seville, Positron emission particle tracking studies of spherical particle motion in rotating drums, Chemical Engineering Science 52 (1997) 2011-2022.